Open Access

CrossMark

Effect of Oxidation Condition on Growth of N: ZnO Prepared by Oxidizing Sputtering Zn-N Film

Xuesi Qin, Guojian Li[*], Lin Xiao, Guozhen Chen, Kai Wang and Qiang Wang

Abstract

Nitrogen-doped zinc oxide (N: ZnO) films have been prepared by oxidizing reactive RF magnetron-sputtering zinc nitride (Zn-N) films. The effect of oxidation temperature and oxidation time on the growth, transmittance, and electrical properties of the film has been explored. The results show that both long oxidation time and high oxidation temperature can obtain the film with a good transmittance (over 80 % for visible and infrared light) and a high carrier concentration. The N: ZnO film exhibits a special growth model with the oxidation time and is first to form a N: ZnO particle on the surface, then to become a N: ZnO layer, and followed by the inside Zn-N segregating to the surface to oxidize N: ZnO. The surface particle oxidized more adequately than the inside. However, the X-ray photoemission spectroscopy results show that the lower N concentration results in the lower N substitution in the O lattice (N_O). This leads to the formation of n-type N: ZnO and the decrease of carrier concentration. Thus, this method can be used to tune the microstructure, optical transmittance, and electrical properties of the N: ZnO film.

Keywords: N-doped ZnO, Film, Oxidation, Growth

Background

Zinc oxide (ZnO) has a wide direct bandgap of 3.4 eV at room temperature and a high exciton binding energy of 60 meV [1]. Additionally, it also has features of being low cost, non-toxic, stable, and transparent [2, 3]. The ZnO film has become one of the most important semiconductor materials and exhibits a wide potential application in the fields of light-emitting diodes [4], spintronic device [5], solar cells [6], thermoelectric materials [7, 8], and so on. As a semiconductor material, it is important to form a p-n junction and to increase the concentration and mobility of a carrier. Now, it has been a challenge to build a high-efficiency and stable homo ZnO p-n junction [9] since the carriers are easy to trap at the p-n heterojunction [10, 11]. Although there are reports about the ZnO homo-junction [12–14], a stable and high-efficiency homo-junction is still in the laboratory research stage. The key point is to prepare p-type ZnO and to improve the concentration and mobility of the carrier.

It is generally recognized that the conductivity type of intrinsic ZnO is n-type because there are many donor impurities that exist, such as oxygen vacancy, zinc interstitial, and hydrogen [1, 15]. Furthermore, the concentration and mobility of the carrier in the n-type ZnO is easy to tune by doping the donor impurity (Al, Ga, In, etc.) [16–18]. However, the dopant of acceptor impurity in ZnO is very difficult [19]. Many elements have been selected as the dopant to obtain a more stable p-type ZnO semiconductor, such as N [20, 21], P [22], As [23], Sb [23], Cu [24], Li [25], Na [26], Ag [27], and Au [28]. In addition, a multi-element co-dopant has also been used to improve the acceptor concentration [29, 30] and to increase the whole concentration so as to compensate the intrinsic defect. But this makes the doping theory become complex. At the same time, the doping result is more difficult to control. Because the elements N and O have similar characters of extranuclear electron structure, ionic radius, and shallow acceptor level, N is one of the more effective dopants for obtaining the p-type ZnO [1–3, 21]. However, the problems of low doping concentration and poor stability still remain for the nitrogen-doped zinc oxide (N: ZnO). The effect of the N dopant and microstructure of the ZnO

* Correspondence: gjli@epm.neu.edu.cn
Key Laboratory of Electromagnetic Processing of Materials (Ministry of Education), Northeastern University, Shenyang 110819, China

Qin *et al. Nanoscale Research Letters* (2016) 11:274

Page 2 of 8

film on the semiconductor properties should be studied further.

In this study, a method has been developed to prepare N: ZnO by thermal oxidation of the reactive radio frequency (RF) magnetron-sputtering zinc nitride (Zn-N) film. Similar oxidation method has been used in our previous studies [31, 32]. That study focuses on the diluted magnetic semiconductor properties of Co: ZnO film by oxidizing a thermal-evaporated Co/Zn bilayer. In this study, the effect oxidation temperature and oxidation time on the crystal structure, surface morphology, chemical state, transmittance, and electrical properties have been studied by using X-ray diffraction (XRD), scanning electron microscopy (SEM), transmission electron microscopy (TEM), X-ray photoemission spectroscopy (XPS), UV–vis spectrophotometry, and the Hall effect measurement. A new growth model of ZnO was found.

Methods

In this study, a Zn-N precursor film was first prepared by reactive RF magnetron sputtering. A high-purity Zn target (99.99 % purity) was used. High-purity N_2 (99.99 %) and Ar (99.99 %) were selected as the sputtering gas. The gas partial pressures are 0.3 and 0.5 Pa for N_2 and Ar, respectively. The base pressure is $<2 \times 10^{-3}$ Pa, and the working pressure is 0.8 Pa. The sputtering time is 15 min. The distance between the target and the substrate is 100 mm. RF sputtering power is 100 W. The substrate temperature remains at room temperature. Monocrystal Si(100) and quartz are selected as the substrate. The substrates are cleaned in an ultrasonic device for 15 min and in turn in acetone and alcohol bath and then dried by high-pressure Ar blowing.
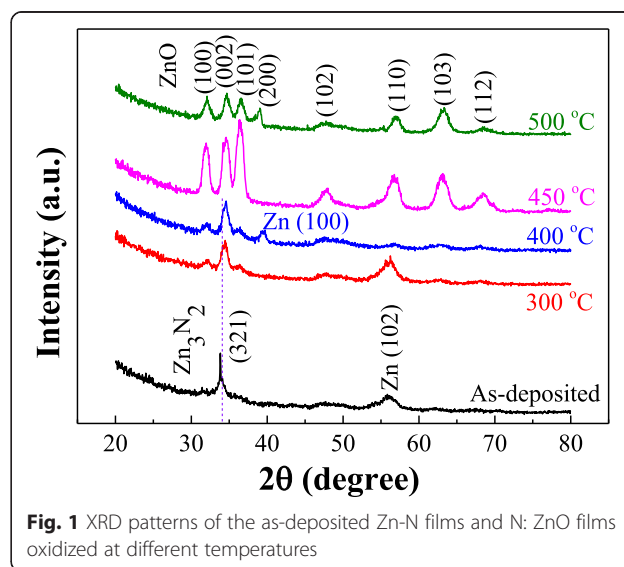
The Zn-N films were then oxidized to become N: ZnO films at air atmosphere in a heat treatment furnace. The Zn-N specimens were put into the furnace when the temperature reached the oxidation temperature, and then, the N: ZnO films were obtained by oxidizing for the desired time. In this study, two series of oxidation conditions were considered. (1) The samples were oxidized for 60 min at different oxidation temperatures of 300, 400, 450, and 500 °C. (2) The samples were oxidized at 400 °C for different times at 30, 60, and 120 min.

The crystal structure of the films was examined by XRD (DMAX 2400, Rigaku) with a grazing incidence of 1° in 2θ mode with monochromatic Cu Kα1 radiation ($\lambda = 0.154056$ nm). Surface morphology was examined by SEM (SUPRA 35, Zeiss). The composition and chemical state of the elements were determined by energy-dispersive X-ray spectroscopy (EDX; Inca, Oxford), XPS (ESCALAB 250Xi, Thermo Scientific), and TEM (2100F, JEOL). Optical transmittance was recorded with a UV–vis spectrophotometer (Lambda 750S, PerkinElmer). The electrical property was investigated by the Hall effect measurements (Ecopia HMS-3000, Korea).

Results and Discussion

In order to confirm the oxidation temperature of ZnO to become transparent for the Zn-N film, the crystal structure and transmittance of the N: ZnO films oxidized at different temperatures for 60 min were first studied. XRD results are shown in Fig. 1. The as-deposited Zn-N film has a (321) peak of Zn_3N_2 and a (102) peak of Zn. This means that the as-deposited film is the coexistence of Zn-N and Zn. Furthermore, the position of the (321) peak agrees well with the result of the others [33]. The intensity is different from the result in Ref. [34] and indicates that the as-deposited film of this study has a good crystallinity. After the oxidation, the peak positions are obviously different from those of the as-deposited and exhibit the characters of ZnO. The intensity of the ZnO peak increases with the temperature. The films oxidized at 300 and 400 °C have the peaks of ZnO and Zn. This means that the films are the coexistence of ZnO and Zn and are not oxidized completely. At the same time, the Zn peak changes to Zn (100) at 400 °C from Zn (102) at 300 °C. According to a previous study [35], the preferred orientation of Zn gradually turns to the orientation of the substrate with the increase of oxidation temperature. In this study, the substrate is Si (100); thus, Zn (102) transformed to Zn (002) when the sample was oxidized at 400 °C for 60 min. This means that the oxidation growth is preferred. Then, only peaks of ZnO exist for the films oxidizing at 450 and 500 °C. The Zn-N films were fully oxidized when the oxidation temperature is ≥400 °C. The crystal structure is wurtzite. However, it can be seen that there is no preferred orientation for the N: ZnO

Fig. 1 XRD patterns of the as-deposited Zn-N films and N: ZnO films oxidized at different temperatures

Qin et al. Nanoscale Research Letters (2016) 11:274

Page 3 of 8

film at 500 °C because the temperature is much higher than the melting point of Zn (420 °C).

SEM was used to analyze the surface morphology of the N: ZnO films, as shown in Fig. 2. Clearly, there are a lot of particles on the surface of the as-deposited Zn-N film. The reason is that some melted droplets of Zn target may be sputtered to the film during the sputtering process because the melting point of Zn is too much low. In addition, there is almost no particle on the surface for the film oxidized at 300 °C. Then, the particle appears again at 400 °C. Moreover, the amount of particles was gradually enhanced with increasing oxidation temperature, and the particles become smaller and aggregate denser. This indicates that the surface morphology can be significantly affected by the oxidation temperature.

Optical transmittance of the N: ZnO films oxidized at different temperatures were measured to confirm whether the transparency can meet the demand and the films are oxidized fully. The results are shown in Fig. 3. The transmittance in the visible and infrared range of the film oxidized at 300 °C is <60 % because much more Zn exists in the film. The transmittance at the visible range of the film oxidized at other temperatures is > 80 % although their surface morphologies are obviously different. The film oxidized at 450 °C has the best transmittance. This means that the higher amount of particles and denser aggregate did not influence the transmittance. The oxidation degree has a significant effect on the transmittance. Too higher oxidation temperature is not good for the transmittance. Therefore, 400 °C was selected as the temperature to consider the effect of oxidation time on the oxidation growth because the oxidation is not complete within 60 min.

Figure 4 shows the XRD patterns of the films oxidized for 30, 60, and 120 min at 400 °C. Clearly, the intensity of ZnO peaks increases with increasing oxidation time. The Zn-N was oxidized completely at 120 min. The position and intensity of the peaks are similar with the film oxidized at 450 °C for 60 min. This indicates that enhancement of both the oxidation temperature and oxidation time can obtain the N: ZnO film with the same crystallinity. Additionally, the XRD peaks of the films oxidized for 30 and 60 min are different. The film oxidized for 30 min has the peaks of ZnO and has no obvious Zn-N and Zn peaks. However, a Zn (100) peak appears for the film oxidized for 60 min. Furthermore, the intensity of the ZnO peaks is also different from that of the peaks oxidized for 30 min. This means that the oxidation growth changes a lot with increasing the oxidation time. More details will be discussed later.

The optical transmittance of the films oxidized for different times at 400 °C is also shown in Fig. 5. It can be seen that the transmittance increases with increasing the oxidation time. The N: ZnO film oxidized for 120 min has the best transmittance (is >80 % in the visible and infrared range) and is similar with the film oxidized for 60 min at 450 °C. The transmittance is strongly related to the oxidation degree. Both long oxidation time and high temperature can obtain films with a good transmittance. Additionally, the transmittance curves of the films oxidized for 30 and 60 min have a plateau region in the 530–650-nm invisible range. This result is similar with those of the films oxidized at different temperatures. This indicates that the oxidation degree plays a key role in influencing the transmittance. However, this is not the point focused by this study.

SEM was used to test the surface morphologies of the N: ZnO films oxidized at 400 °C for different times, as
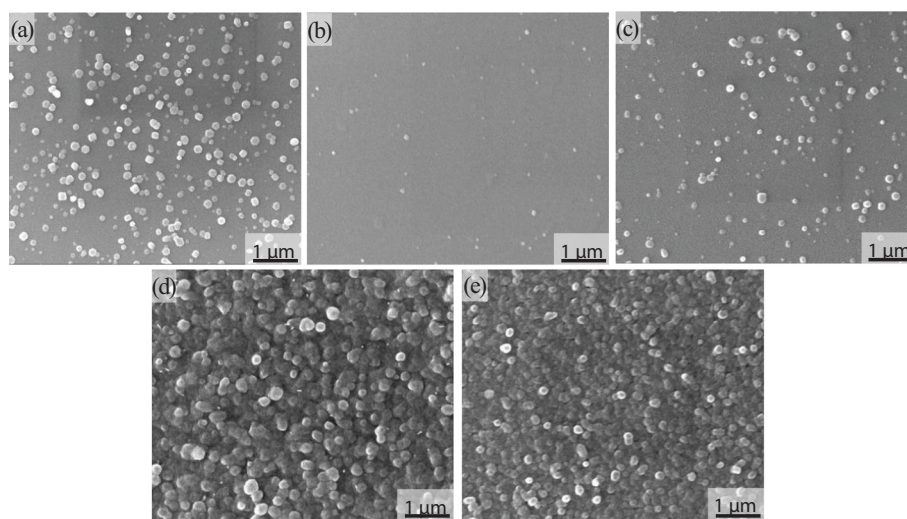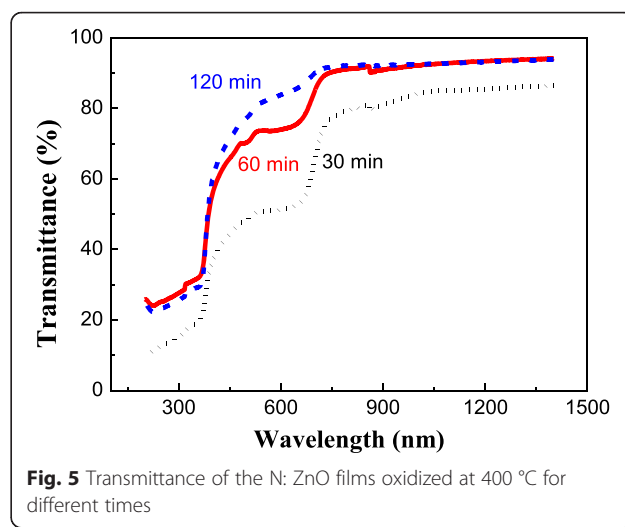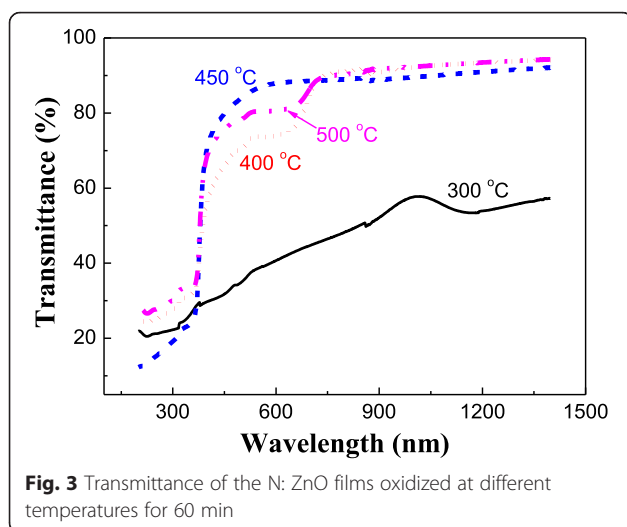

Fig. 2 SEM images of the as-deposited film **a** and the films oxidized at different temperatures of **b** 300, **c** 400, **d** 450, and **e** 500 °C for 60 min

Qin *et al. Nanoscale Research Letters* (2016) 11:274

Page 4 of 8

Fig. 3 Transmittance of the N: ZnO films oxidized at different temperatures for 60 min

Fig. 5 Transmittance of the N: ZnO films oxidized at 400 °C for different times

shown in Fig. 6. It can be seen that the surface is formed by many particles. The amount of the particles on the surface is different for three oxidation times. There are a lot of particles aggregated on the surface of the films oxidized for 30 min. The amount of particles becomes less for 60 min and becomes more for 120 min. Moreover, the surface morphologies of the films oxidized at 300 °C have similar results. The only difference is that the amount of particles is small at a lower oxidation temperature. This indicates that more particles are aggregated on the surface with increasing temperature and time. It is reasonable to conclude that the particle is N: ZnO oxidized by Zn-N. Furthermore, this oxidation growth is significantly different from previous studies [31, 32, 36, 37]. The ZnO grew by forming a dendrite structure in previous studies. This reason may be due to the good crystallinity and existence of a particle on the

Fig. 4 XRD patterns of the N: ZnO films oxidized for different times for 30, 60, and 120 min at 400 °C

surface of the as-deposited Zn-N films. Then, why and how to occur this growth are studied.

The N: ZnO film oxidized at 400 °C for 60 min is an intermediate process of oxidation growth. TEM and SEM were used to study the cross-sectional structure and composition, as shown in Fig. 7. From the TEM result, the film thickness is about 150 nm. There is an amorphous SiO_2 layer at the interface between the Si substrate and the film. The thickness and property of this layer is very important for device application of such a heterostructure film [38]. There exist particles on the surface in both TEM and SEM images. The particle size is about 150–200 nm. The content ratio of Zn to O (Zn/O) at the region from the surface to the inside was tested by EDX of TEM. It can be seen that the Zn/O is about 1:1. The Zn ratio increases from the surface to the inside. This means that the particle on the surface oxidized fully. From the morphology in the yellow box of the SEM image, the shape is similar with a mushroom growth from the soil. Thus, it may be the Zn-N particle that segregated from the bottom.

A growth model was proposed based on the above analysis, as shown in Fig. 8. According to a previous study [39], the ZnO growth started from the apex of Zn during the oxidation process. In this study, the particles on the surface of the as-deposited Zn-N film are first oxidized to become N: ZnO particles. This leads to a lot of aggregated particles that exist on the surface of the films oxidized at 400 °C for 30 min. Then, the oxidized N: ZnO particles continue to oxidize until the N: ZnO becomes a continuous layer. This is the reason why the surface becomes smooth for the film oxidized at 60 min. At the third stage, the inside Zn-N particle in the film segregates the surface of N: ZnO because of the existence of voids in the films, as shown by the bright zone in Fig. 7. Similar phenomena were also found in the
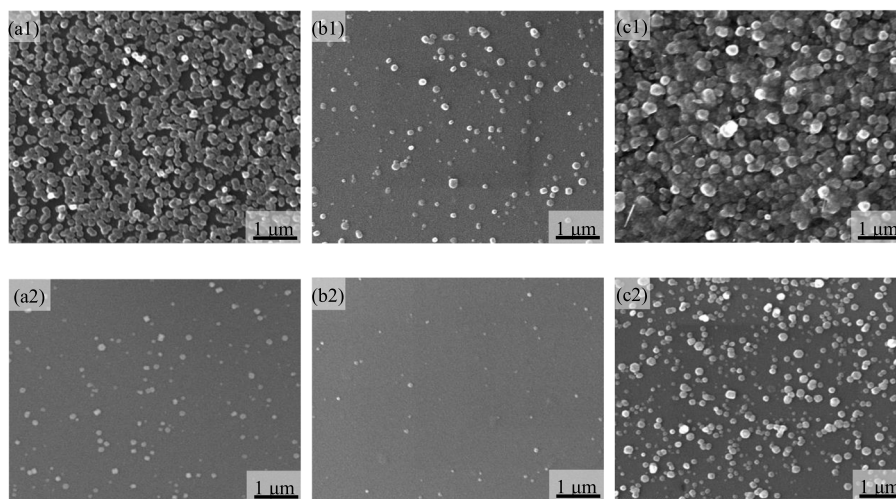
Qin *et al. Nanoscale Research Letters* (2016) 11:274

Page 5 of 8
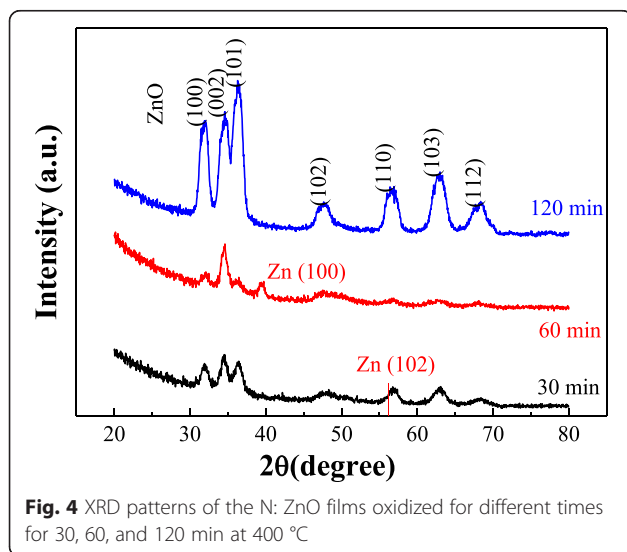
Fig. 6 SEM images of the N: ZnO films oxidized for **a** 30, **b** 60, and **c** 120 min at 400 °C (*top row*) and 300 °C (*bottom row*)

growth of ZnO nanostructures by wet oxidation method [40]. Then, the segregated Zn-N particles were oxidized to become a N: ZnO particle. Thus, a lot of particles aggregated on the surface of the film at 120 min. This leads to the adequate oxidation of the particles on the surface.

XPS was used to examine the composition in depth and the chemical states of the elements. The results are shown in Fig. 9. From the depth profile, it can be seen that Zn, O, and N distribute uniformly in the depth. The Zn content is higher than that of O because the film was not oxidized fully. The N content is very low and about 0.65 %. Additionally, the case of a higher Zn ratio versus O on the surface, as shown in the TEM result, has not appeared in the XPS. This may be because the point to measure the content is not at the particle position during the sputtering measure process. Then, the XPS survey scan spectra with different etching times of 30, 240, and 540 s were used to define the chemical states of the elements, as show in Fig. 9b. Clearly, three peaks have no significant difference. All peaks can be ascribed to

the elements Zn, O, and N. This means that there is no impurity in the film. However, there is an obvious difference for the high-resolution XPS of Si, as show in Fig. 9c. The Si 2p and 2s peaks appear because the Si of the substrate diffuses at the interface of the N: ZnO and Si substrates. This leads to the increase of Si and decrease of Zn and O in the etching time of 400–700 s in Fig. 9a. For the high-resolution XPS of N at 240 s, there are two peaks of N 1s that appear at 396.7 and 405.1 eV [41]. They depict, respectively, the concentration of the N_o acceptor and $(N_2)_o$ double donor. The peak intensity is weak because the content of N is low. Additionally, when the intensity of N_o is much stronger than that of $(N_2)_o$, the N: ZnO film can become n-type.

Then, the Hall effect measurement was used to test the electrical properties of the N: ZnO films oxidized at 400 °C for different times, as shown in Table 1. The Hall coefficients of all the films are negative. This means that all the films are n-type. The p-type N: ZnO was not formed because the N content is too low, as the above analysis of the N XPS result. Furthermore, the carrier
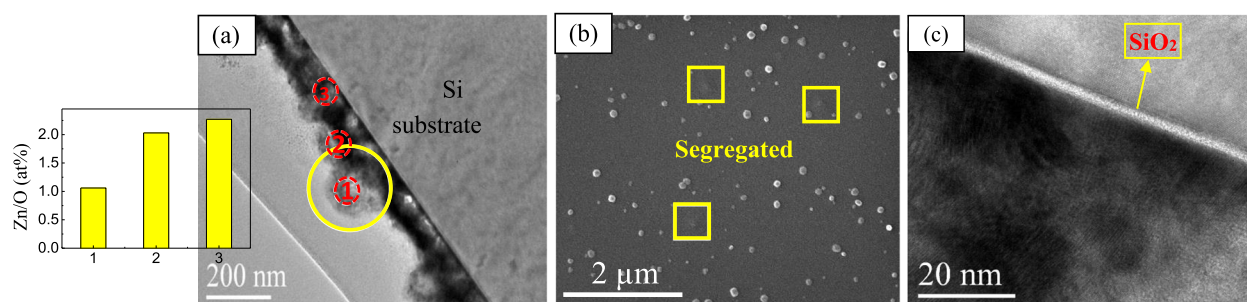

Fig. 7 a Cross-sectional TEM image and content ratio of Zn/O at different regions for the film oxidized at 400 °C for 60 min. **b** SEM morphology of the film. **c** Cross-sectional HRTEM image for the film oxidized at 400 °C for 60 min
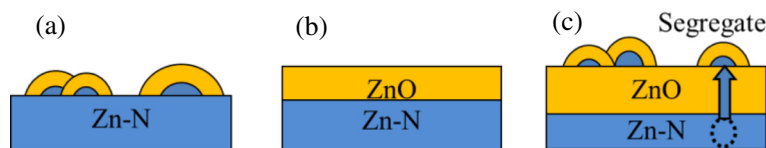
Qin et al. Nanoscale Research Letters (2016) 11:274

Page 6 of 8

Fig. 8 Oxidation growth model of N: ZnO films for different times. **a** Particle on the surface oxidized. **b** Oxidized particles become a N: ZnO layer. **c** Zn-N particles segregate on the N: ZnO surface and oxidized to become a N: ZnO particle

concentration of the film oxidized for 60 min is 2 orders of magnitude lower than the others. The reason may be as follows. For the film oxidized for 30 min, more Zn can provide more carriers. For the film oxidized for 120 min, more O substitution by N can provide more carriers. In addition, the carrier mobility of the film oxidized for 60 min is higher than that of the others. This is because the smooth N: ZnO layer was formed at this stage. This indicates that the aggregation of the N: ZnO particles can deteriorate the carrier mobility because of the scatter of carrier by particle boundaries. This result illustrates that the oxidation method can affect the growth and microstructure. The correlation of structure and electrical properties demonstrates that the oxidation growth gives an effective method to obtain the needed structure and properties of the N: ZnO film.

However, this kind of growth proposes a new method to control the N: ZnO structure. Furthermore, there is a big difference for the carrier concentration and mobility

at different oxidation stages. These provide possibility to prepare p-type ZnO and to improve the concentration and mobility of the carrier. In our study, there are several reasons that lead to the n-type formation and the low carrier concentration and mobility. (1) The substrate temperature maintains at room temperature the deposition of the as-deposited Zn-N film in this study. There are a lot of donor impurities (oxygen vacancy, interstitial zinc, etc.) [42], which lead to a strong self-compensation effect after oxidation. (2) N content is too low. The lower N concentration results in the lower N substitution in the O lattice (N_o). This leads to the formation of n-type N: ZnO and the decrease of carrier concentration. In addition, this leads to the electrical properties of the films which are similar with those of the pure ZnO thin film (n-type) and also the lower carrier concentration [43]. Furthermore, the insulating quartz substrate is nonconductive to generate p-type semiconductors [44].
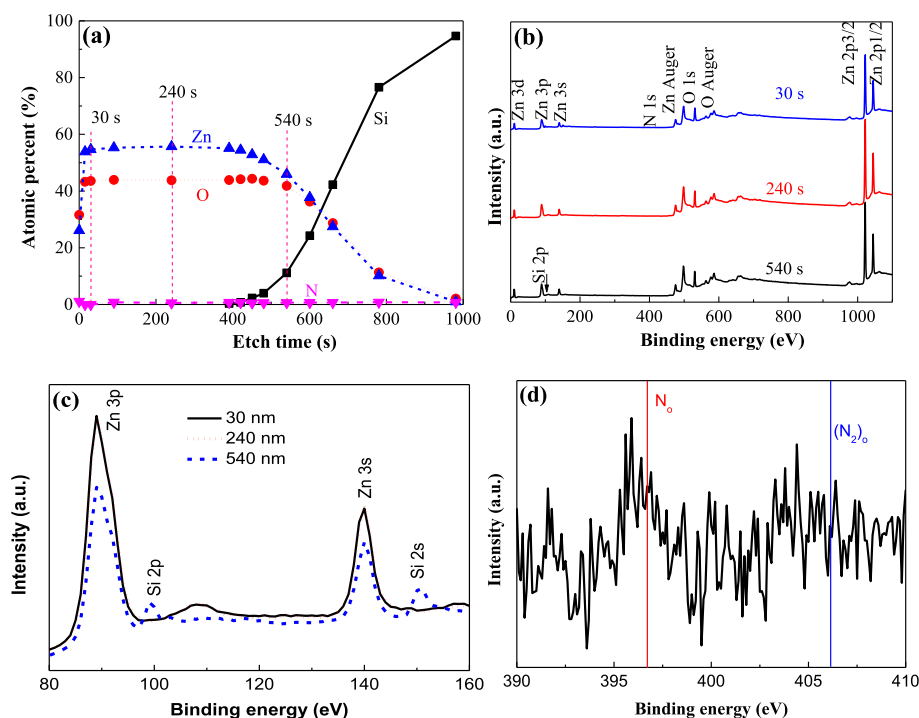

Fig. 9 XPS spectra of N: ZnO film oxidized at 400 °C for 60 min. **a** Depth profile. **b** Survey scan spectra at 30, 240, and 540 s. High-resolution XPS of **c** Si and **d** N at 240 s

Qin *et al. Nanoscale Research Letters* (2016) 11:274

Page 7 of 8

Table 1 Electrical properties of N: ZnO film oxidized at 400 °C for different times

Samples (min)	Resistivity (Ω cm)	Carrier mobility (cm^2/V S)	Concentration (cm^{-3})	Hall coefficient (cm^3/C)
30	7.15	0.92	9.44×10^{17}	−6.61
60	449.7	2.03	6.82×10^{15}	−916.1
120	28.01	1.36	1.64×10^{17}	−38.19

Conclusions

The N: ZnO film was fabricated by the thermal oxidation of the reactive RF magnetron-sputtering Zn-N film. Oxidation temperature and oxidation time have a significant effect on the crystal structure, surface morphology, and chemical state. The correlation of the optical transmittance and electrical properties with the structure was explored. The results show that the control of oxidation condition of N: ZnO film has made the film exhibit a special growth model. The 400 °C temperature and 120 min time is the best oxidation condition for obtaining a high-quality N: ZnO film. The film can be oxidized completely at this condition. Meanwhile, its transmittance is over 85 % for the visible and infrared light and has a higher carrier concentration. The lower N concentration results in the lower N_o substitution in the O lattice. This leads to the formation of n-type N: ZnO and the decrease of carrier concentration. This oxidation growth gives an effective method to obtain the needed structure and properties of the N: ZnO film.

Authors' contributions
XQ and GL designed the experiment and analyzed the results. QW and KW instructed the experimental design. GC performed the experiments and the measurements. LX conducted the SEM and TEM analysis. All authors contributed to compiling the manuscript and have approved it for publication.

Competing interests
The authors declare that they have no competing interests.

References
1. Fan JC, Sreekanth KM, Xie Z, Chang SL, Rao KV (2013) p-Type ZnO materials: theory, growth, properties and devices. Prog Mater Sci 58:874–985
2. Wang M, Ren F, Zhou J, Cai GX, Cai L, Hu YF, Wang DN, Liu YC, Guo LJ, Shen SH (2015) N doping to ZnO nanorods for photoelectrochemical water splitting under visible light: engineered impurity distribution and terraced band structure. Sci Rep 5:12925
3. Stehr JE, Chen WM, Reddy NK, Tu CW, Buyanova IA (2015) Efficient nitrogen incorporation in ZnO nanowires. Sci Rep 5:13406
4. Tsukazaki A, Ohtomo A, Onuma T, Ohtani M, Makino T, Sumiya M, Ohtani K, Chichibu SF, Fuke S, Sgawa Y, Ohno H, Koinuma H, Kawasaki M (2005) Repeated temperature modulation epitaxy for p-type doping and light-emitting diode based on ZnO. Nat Mater 4:42–46
5. Pan F, Song C, Liu XJ, Yang YC, Zeng F (2008) Ferromagnetism and possible application in spintronics of transition-metal-doped ZnO films. Mater Sci Eng R 62:1–35
6. Gonzalez-Valls I, Yu YH, Ballesteros B, Orob J, Lira-Cantu M (2011) Synthesis conditions, light intensity and temperature effect on the performance of ZnO nanorods-based dye sensitized solar cells. J Power Sources 196:6609–6621
7. Nam WH, Lim YS, Choi SM, Seo WS, Lee JY (2012) High-temperature charge transport and thermoelectric properties of a degenerately Al-doped ZnO nanocomposite. J Mater Chem 22:14633–14638
8. Yang Y, Pradel KC, Jing QS, Wu JM, Zhang F, Zhou YS, Zhang Y, Wang ZL (2012) Thermoelectric nanogenerators based on single Sb-doped ZnO micro/nanobelts. ACS Nano 6(8):6984–6989
9. Lim JH, Kang CK, Kim KK, Park IK, Hwang DK, Park SJ (2006) UV electroluminescence emission from ZnO light-emitting diodes grown by high-temperature radiofrequency sputtering. Adv Mater 18:2720–2724
10. Li XY, Chen MX, Yu RM, Zhang TP, Song DS, Liang RR, Zhang QL, Cheng SB, Dong L, Pan AL, Wang ZL, Zhu J, Pan CF (2015) Enhancing light emission of ZnO-nanofilm/Si-micropillar heterostructure arrays by piezo-phototronic effect. Adv Mater 27:4447–4453
11. Schuster F, Laumer B, Zamani RR, Mage'n C, Morante JR, Arbiol J, Stutzmann M (2014) p-GaN/n-ZnO heterojunction nanowires: optoelectronic properties and the role of interface polarity. ACS Nano 8(5):4376–4384
12. Pradel KC, Wu WZ, Ding Y, Wang ZL (2014) Solution-derived ZnO homojunction nanowire films on wearable substrates for energy conversion and self-powered gesture recognition. Nano Lett 14:6897–6905
13. Ko DK, Brown PR, Bawendi MG, Bulovic V (2014) p-i-n heterojunction solar cells with a colloidal quantum-dot absorber layer. Adv Mater 26:4845–4850
14. Li PJ, Liao ZM, Zhang XZ, Zhang XJ, Zhu HC, Gao JY, Laurent K, Wang LY, Wang N, Yu DP (2009) Electrical and photoresponse properties of an intramolecular p-n homojunction in single phosphorus-doped ZnO nanowires. Nano Lett 9(7):2513–2518
15. Rao MSR, Okada T (2014) ZnO nanocrystals and allied materials. Springer India, New Delhi
16. Baek SH, Noh BY, Park IK, Kim JH (2012) Fabrication and characterization of silicon wire solar cells having ZnO nanorod antireflection coating on Al-doped ZnO seed layer. Nanoscale Res Lett 7:29
17. Jun MC, Park SU, Koh J-H (2012) Comparative studies of Al-doped ZnO and Ga-doped ZnO transparent conducting oxide thin films. Nanoscale Res Lett 7:639
18. Thompson RS, Li DD, Witte CM, Lu JG (2009) Weak localization and electron-electron interactions in indium-doped ZnO nanowires. Nano Lett 9(12):3991–3995
19. Dutta S, Chattopadhyay S, Sarkar A, Chakrabarti M, Sanyal D, Jana D (2009) Role of defects in tailoring structural, electrical and optical properties of ZnO. Prog Mater Sci 54:89–136
20. Qin HC, Li WY, Xia YJ, He T (2011) Photocatalytic activity of heterostructures based on ZnO and N-doped ZnO. ACS Appllied Materials & Interfaces 3:3152–3156
21. Zheng M, Wang ZS, Wu JQ, Wang Q (2010) Synthesis of nitrogen-doped ZnO nanocrystallites with one-dimensional structure and their catalytic activity for ammonium perchlorate decomposition. J Nanopart Res 12:2211–2219
22. Kang SJ, Joung YH, Han JW, Yoon YS (2011) Electrical and optical properties of P-doped ZnO thin films by annealing temperatures in nitrogen ambient. J Mater Sci Mater Electron 22:248–251
23. Li WW, Hu ZG, Wu JD, Sun J, Zhu M, Zhu ZQ, Chu JH (2009) Concentration dependence of optical properties in arsenic-doped ZnO nanocrystalline films grown on silicon (100) substrates by pulsed laser deposition. J Phys Chem C 113:18347–18352
24. Suja M, Bashar SB, Morshed MM, Liu JL (2015) Realization of Cu-doped p-type ZnO thin films by molecular beam epitaxy. ACS Appllied Materials & Interfaces 7:8894–8899
25. Chang YT, Chen JY, Yang TP, Huang CW, Chiu CH, Yeh PH, Wu WW (2014) Excellent piezoelectric and electrical properties of lithium-doped ZnO nanowires for nanogenerator applications. Nano Energy 8:291–296

Qin *et al. Nanoscale Research Letters* (2016) 11:274

Page 8 of 8

26. Wang LW, Wu F, Tian DX, Li WJ, Fang L, Kong CY, Zhou M (2015) Effects of Na content on structural and optical properties of Na-doped ZnO thin films prepared by sol-gel method. J Alloys Compd 623:367–373

27. Chen Y, Tse WH, Chen LY, Zhang J (2015) Ag nanoparticles-decorated ZnO nanorod array on a mechanical flexible substrate with enhanced optical and antimicrobial properties. Nanoscale Res Lett 10:106

28. Zhang CL, Shao MF, Ning FY, Xu SM, Li ZH, Wei M, Evans DG, Duan X (2015) Au nanoparticles sensitized ZnO nanorod @ nanoplatelet core-shell arrays for enhanced photoelectrochemical water splitting. Nano Energy 12:231–239

29. Shet S, Ahn KS, Deutsch T, Wang H, Nuggehalli R, Yan Y, Turner J, Al-Jassim M (2010) Influence of gas ambient on the synthesis of co-doped ZnO: (Al, N) films for photoelectrochemical water splitting. J Power Sources 195:5801–5805

30. Bu IYY (2015) Sol-gel synthesis of p-type zinc oxide using aluminium nitrate and ammonia. J Ind Eng Chem 28:91–96

31. Li GJ, Wang HM, Wang Q, Zhao Y, Wang Z, Du JJ, Ma YH (2015) Structure and properties of Co-doped ZnO films prepared by thermal oxidization under a high magnetic field. Nanoscale Res Lett 10:112

32. Li GJ, Wang HM, Zhao Y, Wang Q, Wang K, Wang Z (2015) Effect of oxidation temperature and high magnetic field on the structure and optical properties of Co-doped ZnO prepared by oxidizing Zn/Co bilayer thin films. Mater Chem Phys 162:88–93

33. Sinha S, Choudhury D, Rajaraman G, Sarkar SK (2015) Atomic layer deposition of Zn_3N_2 thin films: growth mechanism and application in thin film transistor. RSC: Advance 5:22712–22717

34. Erdogan NH, Kara K, Ozdamar H, Esen R, Kavak H (2013) Effect of the oxidation temperature on microstructure and conductivity of Zn_xN_y thin films and their conversion into p-type ZnO: N films. Appl Surf Sci 271:70–76

35. Rusu GG, Gîrtan M, Rusu M (2007) Preparation and characterization of ZnO thin films prepared by thermal oxidation of evaporated Zn thin films. Superlattice Microst 42:116–122

36. Li ZW, Gao W, Reeves RJ (2005) Zinc oxide films by thermal oxidation of zinc thin films. Surf Coat Technol 198:319–323

37. Shao LX, Zhang J (2008) A simple preparation technique of ZnO thin film with high crystallinity and UV luminescence intensity. J Phys Chem Solids 69:531–534

38. Zhang K, Kim SJ, Zhang Y, Heeg T, Schlom DG, ShenW Z, Pan X (2014) Epitaxial growth of ZnO on (111) Si free of an amorphous interlayer. J Phys D Appl Phys 47:105302

39. Kim TW, Kawazoe T, Yamazaki S, Ohtsu M, Sekiguchi T (2004) Low-temperature orientation-selective growth and ultraviolet emission of single-crystal ZnO nanowires. Appl Phys Lett 84:3358–3360

40. Chen R, Zou C, Yan X, Alyamani A, Gao W (2011) Growth mechanism of ZnO nanostructures in wet-oxidation process. Thin Solid Films 519:1837–1844

41. Lin CW, Song YP, Chang SC (2015) Rapid thermal oxidation of zinc nitride film. Jpn J Appl Phys 54:04DH06

42. Wang J, Sallet V, Jomard F, Rego AM, Elamurugu E, Martins R, Fortunato E (2007) Influence of substrate temperature on N-doped ZnO films deposited by RF magnetron sputtering. Thin Solid Films 515:8785–8788

43. Allenic A, Guo W, Chen Y, Katz MB, Zhao G, Che Y, Hu Z, Liu B, Zhang SB, Pan X (2007) Amphoteric phosphorus doping for stable p-type ZnO. Adv Mater 19:3333–3337

44. Ye HB, Kong JF, Pan W, Shen WZ, Wang B (2009) Multi-carrier transport properties in p-typ e ZnO thin films. Solid State Commun 149:1628–1632